

ACCRETION MODES IN COLLAPSARS - PROSPECTS FOR GRB PRODUCTION

WILLIAM H. LEE

Instituto de Astronomía, Universidad Nacional Autónoma de México, Apdo. Postal 70-264, Cd. Universitaria, México D.F. 04510:wlee@astroscu.unam.mx

AND

ENRICO RAMIREZ-RUIZ*

School of Natural Sciences, Institute for Advanced Study, Princeton, NJ, 08540: enrico@ias.edu

Draft version January 25, 2020

ABSTRACT

We explore low angular momentum accretion flows onto black holes formed after the collapse of massive stellar cores. In particular, we consider the state of the gas falling quasi-spherically onto stellar-mass black holes in the hypercritical regime, where the accretion rates are in the range $10^{-3} \lesssim \dot{M} \lesssim 0.5 M_{\odot} \text{ s}^{-1}$ and neutrinos dominate the cooling. Previous studies have assumed that in order to have a black hole switch to a luminous state, the condition $l \gg r_g c$ needs to be fulfilled. We argue that flows in hyperaccreting, stellar mass disks around black holes are likely to transition to a highly radiative state when their angular momentum is just above the threshold for disk formation, $l \sim 2r_g c$. In a range $r_g c < l < 2r_g c$, a *dwarf* disk forms in which gas spirals fast into the black hole without any help from horizontal viscous stresses due to general relativistic effects. For high rotation rates $l \geq 2r_g c$, the luminosity is supplied by large, hot equatorial bubbles around the black hole. The highest neutrino luminosities are obtained for $l \approx 2r_g c$, and this value of angular momentum also produces the most energetic neutrinos, and thus also the highest energy deposition rates. Given the preferential range of l explored in this work, we argue that, as long as $l \geq 2r_g c$, low angular momentum cores may in fact be better suited for producing neutrino-driven explosions following core collapse in supernovae and γ -ray bursts.

Subject headings: accretion, accretion disks — dense matter — hydrodynamics — gamma rays: bursts — supernovae: general

1. INTRODUCTION

The collapse of massive cores in evolved stars is clearly one of the most energetic events in astrophysics, producing observable electromagnetic, neutrino, and, in all likelihood, gravitational signatures. When it was discovered that the accretion shock launched from the proto-neutron star after core bounce would stall under a wide range of conditions, energy transfer from the proto-NS to the outer regions through neutrinos was invoked as a possible mechanism to re-energize the shock wave and explode the star (Bethe & Wilson 1985). The failure to reach a consensus regarding the physics involved in a successful explosion in spherical symmetry (Burrows & Thompson 2003) has led to the exploration of many possible channels and physical mechanisms to transfer energy to the shock and launch a supernova.

The rotation and magnetic field of the progenitor and the newborn compact object are important ingredients for a global understanding the explosion mechanism (LeBlanc & Wilson 1970; Wheeler, Meier & Wilson 2002; Akiyama et al. 2003; Ardeljan, Bisnovati-Kogan & Moiseenko 2005; Thompson, Quatern & Burrows 2005; Wilson, Mathews & Dalhed 2005) and the subsequent evolution of the system, as is convection (Janka & Müller 1996). Recent studies have addressed these issues in two (Fryer & Heger 2000) and three dimensions (Fryer & Warren 2004; Janka et al. 2005), although a definitive conclusion is still not available. Any of these effects may enhance the effective neutrino luminosity in the inner regions and thus power the explosion. Implications range from the success or failure of the explosion itself, the possible production of a classical γ -ray burst, the imparted kick to the newborn neutron star or black hole, and the generation of a strong gravitational wave signal.

Unfortunately, determining the precise manner in which a star is rotating is extremely complicated, depending upon evolutionary details such as mass loss from the main-sequence star and the configuration of the magnetic field, to name but two issues (Spruit 2002; Heger et al. 2005) which lead to substantial core spin-down in late evolutionary phases. Binary interactions may also clearly affect the angular momentum of a star prior to core collapse, through spin-up torques by tidal interactions.

In the context of GRBs, the collapsar model (Woosley 1993) invokes the formation of a massive accretion disk around a newborn black hole through fall-back accretion after core collapse. The energy release associated with the huge accretion rates (of order 0.1 solar masses per second) may be sufficient, if focused along the rotation axis of the star, to produce a GRB. The angular momentum of the infalling gas is an important parameter in this case, since it determines if a disk will form (if there is no rotation only Bondi-like accretion will ensue) and its dimensions when it does. The accretion disk is likely to be small enough that general relativity will play an important role in its inner regions, allowing accretion even for finite values of angular momentum, as will be discussed below. A critical concern when assessing the viability of progenitors for the production of GRBs has thus been their rotation rate, as can best be determined from stellar evolution considerations. We note here that Woosley & Heger (2005) and Yoon & Langer (2005) have recently pointed out a new evolutionary channel for very massive stars, in which mass and associated angular momentum losses are greatly reduced by thorough mixing on the main sequence and the subsequent avoidance of the giant phase. Previous work in collapsar models and the associated neutrino-cooled accretion flows (MacFadyen & Woosley

* Chandra Fellow

1999; Popham, Woosley & Fryer 1999; Narayan, Piran & Kumar 2001) has generally considered relatively high rotation rates and associated angular momentum values, typically with $l \approx 6r_g c$. With these values large, centrifugally supported disks several hundred kilometers across promptly form around the newborn black hole.¹ In this paper we consider a wide range of rotation rates, covering cores with near radial inflow to values slightly below those usually considered in collapsar calculations. In the low-angular momentum limit, we find that considerable energy release is still possible, and could contribute significantly to the energy release available for a GRB. Some elements of this picture have been considered in a quite different context before, namely High-Mass X-ray Binaries, and we draw some analogy and useful comparisons from this. In § 2 we detail the consequences of angular momentum on the flow of collisionless matter, and note the regime where hydrodynamics comes into play. A presentation of the different accretion modes that occur, depending on whether angular momentum transport plays a role or not is made in § 3. We conclude in § 4 with a discussion on the prospects for GRB production from such systems.

2. THE CONSEQUENCES OF ANGULAR MOMENTUM

Before proceeding to the particular results of this set of calculations, relevant for collapsars, this section is devoted to more general considerations. The reader may wish to also consult the clear introductory exposition by Beloborodov & Illiaronov (2001).

2.1. Flow lines for ballistic parabolic motion

Consider purely ballistic motion of collisionless matter with zero energy in the gravitational potential well of a central mass, M . In Newtonian theory, a test mass will follow a parabolic trajectory, uniquely determined by its angular momentum, l . If the central mass is a mathematical point, this will occur for any value of l . In a realistic astrophysical situation, the mass M has a finite radius R , so capture orbits exist whenever the periastron distance is smaller than R . One may term accretion in such a situation “direct accretion”, or accretion by capture. The effective cross section of the mass M for this capture, $\sigma_{\text{Newt}} = \pi R^2 (1 + 2GM/v_\infty^2)$, where v_∞ is the particle’s velocity far from the mass M , is larger than the physical cross section, $\sigma = \pi R^2$, because of gravitational focusing (Shapiro & Teukolsky 1983).

In general relativity (GR), there is an additional effect, because the centrifugal barrier disappears even for finite l . Any particle with enough energy at a given angular momentum will inevitably fall onto the central mass. For definiteness, if $l = 2r_g c$, the effective potential exhibits a local maximum at $r = 4GM/c^2$ (where an unstable, marginally bound circular orbit is possible). A particle in this situation with energy $E > 0$ may thus directly accrete. Capture orbits are thus of a different nature than in Newtonian theory, and the effective cross section for this to occur may be written as $\sigma_{\text{GR}} = 4\pi(2M)^2/v_\infty^2$, which corresponds to a critical angular momentum $l_{\text{crit}} = 4GM/c$.

Consider now a situation in which a rotating cloud of particles, with angular momentum about the z -axis, enshrouds a central black hole of mass M . For vanishing particle energy, these will be in near free-fall and follow approximately parabolic orbits. For a monotonically increasing distribution of l with the polar angle θ , particles closer to the poles will fall more easily than those along the equator. We may divide the trajectories into three categories, shown in Figure 1: (a) those that accrete directly; (b) those that would accrete onto the black hole directly, but cross the equatorial plane, $z = 0$, before they are able to do so; and (c) those that encounter their circularization radius (where the centrifugal force balances gravity) on the equatorial plane and will not accrete directly if the equatorial angular momentum is high enough. Lines of type (b) coming from one hemisphere in fact encounter an approaching line from the opposite direction. If the energy in vertical motion is dissipated efficiently (through radiation) a thin disk will form. The material in this disk does not have sufficient angular momentum to remain in orbit, and will thus fall onto the central mass in a short timescale, even in the absence of any mechanism that transports angular momentum. This particular scenario, with Compton cooling in mind, was applied by Beloborodov & Illiaronov (2001) in the context of high-mass X-ray binaries (HMXBs). That the flow lines corresponding to ballistic motion do indeed cross obviously indicates that a shock will form, and that a full analysis requires the inclusion of hydrodynamical effects.

2.2. Hydrodynamical effects

Initially, a shock will form in the equatorial plane, $z = 0$, and the energy in vertical motion will be transformed into internal energy. If cooling occurs, some of this will be lost from the system (through photons or neutrinos, depending on the physical conditions). If the cooling rate \dot{q} is able to balance the energy input behind the shock front, the disk will remain geometrically thin, with a scale height $H \ll r$. The fluid will then orbit the central mass until it reaches a circular orbit corresponding to its angular momentum. In Newtonian theory, this is the circularization radius $r_c = l^2/GM$. Thereafter, if angular momentum is removed, it may slowly accrete onto the central mass through a sequence of quasi-Keplerian orbits. In the case of a relativistic potential, as considered here, only the orbits of type (c) described in § 2.1 will be like this. Type (b) trajectories will remain in the equatorial plane after passing through the shock front, but the fluid along them will never find a proper circularization radius, because of its low value of angular momentum. This will form the fast, inviscid and near free-fall disk envisaged by Beloborodov & Illiaronov (2001).

If the cooling mechanism is not so efficient, and is unable to dissipate all the internal energy generated at the shock, a hot toroidal bubble will form and grow in the equatorial plane. Its size and stability depend on several factors. The first of these is simply the total energy input, fixed by the accretion rate at the outer boundary. The second is the cooling rate, given by the relevant electromagnetic and neutrino processes (in the context of collapsars only neutrino cooling plays a role). If the cooling rate does not drop precipitously with decreasing density or temperature, the bubble may eventually stabilize and reach a stationary configuration. A larger bubble offers a larger volume within which to dissipate the internal energy produced at the shock. The

¹ The production of magnetically driven outflows has been considered as well, see Proga et al. (2003)

third is the geometry of injection at the outer boundary, which directly affects the flow. For example, if the injection is restricted to the equatorial plane (Chen et al. 1997; Igumenshchev & Abramowicz 1999), polar outflows may appear, which transport energy from the equatorial regions to higher latitudes. Finally, the efficiency of angular momentum transport may cause enough advection of matter and its accompanying internal energy so as to stabilize the flow, or at least keep the bubble below a certain maximum size, even if it is variable on short timescales. For the case of inviscid hydrodynamic accretion, Proga & Begelman (2003a) have showed that the formation of a hot torus directly affects the accretion rate onto the central object. The fluid that would otherwise reach the equator at large radii is deflected by the torus into a narrower funnel close to the rotation axis.

Considering these further complexities, namely: (i) “partial” cooling, in which not all the internal energy generated at the shock is removed from the system and (ii) a finite optical depth, which acts in a similar way, it is clear that a full analytic solution cannot be obtained, and that numerical calculations are necessary to study this scenario.

2.3. Input physics and initial conditions

We believe the following assumptions will not alter the significance of our overall results. We assume azimuthal symmetry and perform our calculations in cylindrical (r, z) coordinates. This allows for greater spatial resolution than a 3D calculation and a solid discussion of angular momentum effects. We do *not* assume reflection symmetry with respect to the equatorial plane. We take the fall back fluid to be in free-fall (i.e. on parabolic orbits) in the central potential well of the black hole and superimpose on it an angular momentum distribution corresponding to rigid-body rotation, $l = l_0 \sin^2 \theta$, where θ is the polar angle, measured from the rotation axis. l_0 is small compared to the local Keplerian value needed to maintain a circular orbit, so it is nearly in free-fall. Capture orbits are an essential ingredient in this model, so we use the formula of Paczyński & Wiita (1980) for the gravitational potential of the black hole, $\Phi = -GM_{\text{BH}}/(r - r_g)$, where $r_g = 2GM_{\text{BH}}/c^2$ is the Schwarzschild radius.

We consider an equation of state with contributions from radiation, relativistic electron–positron pairs and non-degenerate α particles and free nucleons. For the latter, we assume nuclear statistical equilibrium and calculate the mass fraction of photodisintegrated nuclei as (Qian & Woosley 1996):

$$X_{\text{nuc}} = 22.4 \left(\frac{\rho [\text{g cm}^{-3}]}{10^{10}} \right)^{-3/4} \left(\frac{T [\text{K}]}{10^{10}} \right)^{9/8} \exp(-8.2 \times 10^{10}/T [\text{K}]). \quad (1)$$

If this expression results in $X_{\text{nuc}} \geq 1$ we set $X_{\text{nuc}} = 1$. The pressure is given by:

$$P = \frac{11}{12} a T^4 + \left(\frac{1 + 3X_{\text{nuc}}}{4} \right) \frac{\rho k T}{m_u}, \quad (2)$$

where all the symbols have their usual meanings. Although in the higher density regions neutronization may lower the electron fraction, we assume here for simplicity that $Y_e = 0.5$ remains constant.

The gas is opaque to electromagnetic radiation, and the main source of cooling (other than advection into the black hole) is neutrino emission. Given the high temperatures and the degree of photodisintegration, the dominant terms arise from e^\pm annihilation and e^\pm capture by free nucleons. The corresponding cooling rates (consistently with the equation of state) are then (Kohri & Mineshige 2002; Itoh et al. 1989)

$$\dot{q}_{\text{cap}} = X_{\text{nuc}} 9.2 \times 10^{33} (T [\text{K}] 10^{11})^6 \frac{\rho [\text{g cm}^{-3}]}{10^{10}} \text{erg cm}^{-3} \text{s}^{-1}, \quad (3)$$

and

$$\dot{q}_{\text{pair}} = 4.8 \times 10^{33} \left(\frac{T [\text{K}]}{10^{11}} \right)^9 \text{erg cm}^{-3} \text{s}^{-1}. \quad (4)$$

Nucleon–nucleon bremsstrahlung neutrino emission is also included in the code, but is insignificant compared with the other two. Photodisintegration of α particles is also taken into account in the energy equation (see Lee, Ramirez–Ruiz & Page 2005). The densities and temperatures do not rise enough for the gas to be optically thick to neutrinos, i.e. $\tau_\nu \ll 1$ always (this is estimated by considering coherent scattering off free nucleons and α particles). Thus all the energy in the form of neutrinos is lost immediately, and the cooling is extremely efficient in this respect. The hydrodynamics is followed using a 2D Smooth Particle Hydrodynamics code (Lee & Ramirez–Ruiz 2002; Lee, Ramirez–Ruiz & Page 2004), which includes all the terms from the viscous stress tensor and uses an α –prescription for the magnitude of the viscosity, $\nu = c_s^2 \alpha / \Omega_k$ (c_s is the local sound speed and Ω_k is the Keplerian angular velocity).

3. ACCRETION MORPHOLOGIES AND LUMINOSITIES

We now address the particular case of accretion following core collapse in massive stars within the previous context. The relevant parameters for a calculation are the equatorial angular momentum, l_0 , the viscosity α , the accretion rate at the outer boundary, \dot{M} , and the location of the boundary itself, typically at $50r_g$ (although for the highest values of angular momentum we explored it was placed at $80r_g$). We have concentrated on variations in the $l_0 - \alpha$ plane for various values of \dot{M} . For all the calculations presented here, the central black hole is assumed to contain $M_{\text{BH}} = 4M_\odot$.

3.1. Low angular momentum – Dwarf Disks

If the angular momentum of the infalling gas is low, a substantial fraction of the fluid is accreted directly onto the black hole, and the rest produces an equatorial shock, where the energy in vertical motion goes into thermal energy. It is efficiently radiated

away in neutrinos (recall that the densities are not high enough for neutrino opacities to play any role), and a thin, dwarf disk forms. The actual simulation looks very much like the analytical streamlines for collisionless matter plotted in Figure 1. After an initial transient lasting $\approx 200r_g/c \approx 6$ ms (corresponding to the free-fall time of the material that is close to the black hole), the system reaches a stationary state, in which as much energy is dissipated in the shock as is radiated in neutrinos.

The steady, low-angular momentum flow configuration is insensitive to the actual value of the viscosity parameter that is used. For a calculation with $l_0 = 1.9r_g c$, behaving as just described, the results are identical whether $\alpha = 0$ or $\alpha = 0.1$ (see Figure 2). The system is in the *inviscid* regime, in which accretion onto the central mass is driven by general relativistic dynamical effects, and not by the transport of angular momentum. In the Newtonian regime this solution is non-existent because of the lack of capture orbits for finite l .

The neutrino luminosity as a function of time is fairly constant, although fast variations at small amplitude are apparent. Part of this variability is of numerical origin, because the equatorial dwarf disk is so thin that it is difficult to resolve adequately (the noise level decreases if the resolution of the calculation is increased). The density in this type of flow is essentially given by the free-fall type conditions and mass conservation through the continuity equation, as

$$\rho \approx \frac{\dot{M}}{4\pi r^2 v_r} = \frac{\dot{M}}{4\pi r_g^2 c} \left(\frac{r}{r_g}\right)^{-3/2} = 2 \times 10^9 \left(\frac{\dot{M}}{0.5M_\odot s^{-1}}\right) \left(\frac{r}{r_g}\right)^{-3/2} \text{ g cm}^{-3} \quad (5)$$

for $M_{\text{BH}} = 4M_\odot$. The crucial difference from spherical Bondi-type accretion is in the formation of the equatorial shock because of the finite, albeit small, value of angular momentum, which raises the temperature to $\approx 3-4$ MeV. Thermal effects dominate, and the mean neutrino energy is accordingly of order $E_\nu \approx kT$.

3.2. High angular momentum – Toroidal Bubbles

For high values of l_0 , the material closest to the equator has enough angular momentum to remain in stable circular orbit around the black hole. We first consider $\dot{M} = 0.01M_\odot s^{-1}$, and defer higher accretion rates to § 3.3. A shock initially forms close to the circularization radius, and the energy in free-fall is transformed into internal energy. The temperature and density in the gas rise rapidly behind the shock front, to a few $\times 10^{11}$ K, and $\approx 10^7 - 10^9$ g cm $^{-3}$, depending on the assumed value of \dot{M} . A hot toroidal bubble is promptly formed and intense neutrino emission takes place within it (see Figure 3). The material is rapidly photodisintegrated into nucleons and protons after passing through the shock, and e^\pm annihilation and capture onto free nucleons contribute to the total neutrino luminosity. The global behavior of the accretion flow depends essentially on the efficiency of angular momentum transport, and also on the accretion rate. For high viscosities ($\alpha = 0.1$), the gas is accreted efficiently so that the growth of the bubble is slower, and the total neutrino luminosity is *lower* by about a factor of 2 with respect to the inviscid ($\alpha = 0$) case. This comes about because: (i) a large fraction of the bubble is hot enough to radiate copious amounts of neutrinos, and high viscosity implies a smaller radiating volume due to the efficient transport of angular momentum (see Figure 4); and (ii) more efficient angular momentum transport means that less matter accumulates in the equatorial region inside the bubble, and thus less energy is released in neutrinos. Note that the fact that a higher viscosity also implies a greater amount of dissipated energy does not reverse this trend.

The neutrino luminosity for $l_0 = 2.1r_g c$ and $\dot{M} = 0.01M_\odot s^{-1}$ as a function of time is shown in Figure 5. There are large-amplitude fluctuations, due to variations in the size, shape and structure of the growing toroidal bubble. Changes by up to a factor of two occur over a background emission rate that is fairly steady, and on a timescale $\Delta t \approx r_b/c_s$, where $r_b \approx 20r_g$ is the size of the hot bubble, and c_s is the sound speed. The temperature is typically $T \approx 10^{10}$ K, so this gives $\Delta t \approx 2$ ms, in rough agreement with the observed variability timescale of $\approx 150r_g/c = 4-5$ ms. Most of the emission arises from the innermost equatorial regions, and it is changes in this volume that affect the total luminosity.

In the inviscid limit there is no angular momentum transport, and so a substantial fraction of the matter cannot accrete. The toroidal bubble thus grows, fluctuating on short timescales and eventually becoming as large as the computational domain (at which point the calculation is stopped). We note that outflows are ubiquitous in this case, as they are a natural way of transporting the stored energy to larger radii. Their detailed analysis is beyond the scope of this paper and is left for future work. If the viscosity is finite, however, the bubble eventually reaches a steady state, in which the accretion by angular momentum transport is balanced by the mass and energy inflow at the outer boundary.

For a given magnitude of the viscosity, the size of the bubble depends on the equatorial angular momentum, l_0 . The circularization radius R_c for matter falling along $z = 0$ (in the pseudo-Newtonian potential is determined by the condition $R_c^3/[R_c - r_g] = l_0^2/GM_{\text{BH}}$), and gives a first estimate of the shock location. All other things being equal, at large angular momentum the torus will be larger, and of lower density and temperature. Despite the larger neutrino-emitting volume and due to the steep dependence of the cooling rates on the temperature, for a fixed magnitude of the viscosity, larger tori have lower luminosities.

3.3. Varying the accretion rate

We have considered variations in the accretion rate by computing models with $\dot{M} = 10^{-3}, 10^{-2}, 10^{-1}, 5 \times 10^{-1} M_\odot s^{-1}$. An increase by one order of magnitude affects the density by about the same amount, simply because of mass conservation. The temperature also rises, but only about $10^{1/4}$ per order of magnitude increase in density. Since the neutrino emission rates from pair capture and annihilation scale as T^9 and ρT^6 respectively, the total luminosities should increase by $\approx 10^{2.5}$ and $10^{2.25}$. So the total change, is by a factor $\approx 10^{2.5}$. Indeed this is what is seen when the actual values for L_ν are computed, so that at a fixed l_0 , $L_\nu \propto \dot{M}^{2.5}$. At very high accretion rates the pre-shock region is dense and cold enough that degeneracy effects start to become important. The post-shock region, however, is always hot enough that our assumptions concerning the equation of state are still valid.

For the highest accretion rates, $\dot{M} \simeq 0.1 - 0.5 \text{ M}_\odot \text{ s}^{-1}$, likely to occur in the initial stages of fallback following the formation of the black hole, the solution changes quantitatively from that described above in § 3.2, because of the increased density. The annihilation of e^\pm is essentially a thermal process, and as such its emissivity depends only on the temperature, while pair capture onto free nucleons involves interactions with the background fluid, making the emissivity proportional to the density. As the density increases, pair capture becomes increasingly important until it eventually dominates the total cooling rate by a factor four at $\dot{M} = 0.5 \text{ M}_\odot \text{ s}^{-1}$, and making it proportionally larger than for lower accretion rates. This is illustrated in Figure 6, where the differential and integrated neutrino luminosities are shown for two different accretion rates at the same equatorial angular momentum (separated into the two main processes contributing to the cooling rate). The net result is that calculations without efficient transport of angular momentum reach higher densities and emissivities, and thus produce smaller equatorial bubbles than if viscosity is present (see Figure 7).

As for lower accretion rates, with finite viscosity the hot torus eventually stabilizes, with a total volume determined by the equatorial angular momentum. Figure 8 shows the radial run of several variables along $z = 0$ for such a stable configuration. The accretion shock is clearly seen as a large jump in density and temperature. Within the torus, the rotation curve is nearly Keplerian, and the radial velocity shows variations due to the stable, large scale circulation pattern that is established and maintained (see Figures 3 and 7). These solutions are similar to those obtained analytically by Popham, Woosley & Fryer (1999) and numerically by MacFadyen & Woosley (1999) and Proga et al. (2003). In the region exterior to the shock front they differ because we have assumed pure free fall, whereas their models consider either an extended Keplerian disk or an actual infalling stellar envelope with substantial pressure support. This effective boundary condition has little effect on the structure and evolution of the inner accretion flow.

Further insight can be gained about the structure of the flow by plotting the density as a function of the temperature (see Figure 9). The location of the shock, the corresponding transition from α particles to free nucleons because of photodisintegration, and the relative importance of neutrino emission in different regions are clearly seen. Larger equatorial bubbles are also more diluted, so the maximum density slowly decreases with increasing angular momentum. For much higher densities the effects of degeneracy and neutronization become more important, and the equation of state would need to be modified.

Regardless of the accretion rate, when the system enters the *inviscid* regime in the low angular momentum limit, L_ν becomes independent of α and the luminosity drops rapidly. This can be seen in the large panel in Figure 9 where we plot the luminosity as a function of the equatorial angular momentum l_0 for inviscid and viscous calculations at high and low accretion rates. The joining of the two classes of solutions at $l_0 \approx 2r_g c$ marks the transition to inviscid accretion and the appearance of the dwarf disk in near free-fall. For $l_0 < 2r_g c$, $L_\nu \propto l_0^{16}$, reflecting the fact that a large fraction of the infalling material is directly accreted by the black hole, and thus the rapid shutoff as the angular momentum is decreased. In the opposite case we find $L_\nu \propto l_0^{-2}$, because larger toroidal bubbles are less dense and have lower temperatures than smaller ones. Combining all of these results, we find that the neutrino luminosity can be fitted piecewise as:

$$L_\nu \approx \begin{cases} 8 \times 10^{50} \left(\frac{l_0}{1.9r_g c} \right)^{16} \left(\frac{\dot{M}}{0.5 \text{ M}_\odot \text{ s}^{-1}} \right)^{2.5} \text{ erg s}^{-1} & \text{for } l_0 \leq 2r_g c \\ 10^{52} \left(\frac{l_0}{2.2r_g c} \right)^{-2} \left(\frac{\dot{M}}{0.5 \text{ M}_\odot \text{ s}^{-1}} \right)^{2.5} \text{ erg s}^{-1} & \text{for } l_0 \geq 2r_g c. \end{cases} \quad (6)$$

3.4. Neutrino spectrum and energy deposition

The shifting contributions to the cooling rate from different processes as the accretion rate increases will affect the emergent neutrino spectrum. Neutrinos produced by pair annihilation have energies $E_\nu \approx kT$. If degeneracy effects are important, those arising from pair capture will have energies comparable with the electron Fermi energy, and one can show that $E_\nu \approx 9(\rho_{10} Y_e)^{1/3} \text{ MeV}$. For the models we have computed with the highest accretion rates this is indeed the case. With these two expressions we have computed the neutrino energies for models with $\dot{M} = 0.5 \text{ M}_\odot \text{ s}^{-1}$ (see Table 1) as a function of the equatorial angular momentum, l_0 . Changing l_0 by only a factor of a few can have a dramatic consequence on the energies of the emitted neutrinos. Moreover, since the energy deposition rates from $\nu\bar{\nu}$ annihilation scale as $Q_{\nu\bar{\nu}} \propto E_\nu^2$, this can have a profound impact on the associated outflows. (Ramirez-Ruiz & Socrates 2005) — from $l_0 = 3r_g c$ to $2.1r_g c$ the rate will increase by a factor 7.5.

3.5. Accompanying winds, supernovae and γ -ray bursts

The high neutrino fluxes ablate baryonic material from the surface of the disk. The properties of such winds, arising from proto-neutron stars following core-collapse, have been investigated before in spherical symmetry (Qian & Woosley 1996). With the typical numbers from our simulations, we find that the mass outflow rate will be approximately

$$\dot{M}_b \sim 5 \times 10^{-4} \left(\frac{L_\nu}{10^{52} \text{ erg s}^{-1}} \right)^{5/3} \text{ M}_\odot \text{ s}^{-1}. \quad (7)$$

Most of the ablation is due to the absorption on nucleons. These outflows are relatively slow. Even the gas that is ejected from the innermost region of the disk has a speed of only $\sim 0.1c$; the gas that comes out from larger radii is even slower. At $L_\nu \sim 3 \times 10^{52} \text{ erg s}^{-1}$, the ablation rate in equation (7) is up to ~ 10 times higher than what can be driven, on energetic grounds, by $\nu\bar{\nu}$ annihilation alone. To see this, combine the lower bound to the photon-pair flux estimated by the reaction $\nu + \bar{\nu} \rightarrow e^+ + e^-$, which yields $L_{\nu\bar{\nu}} \sim 10^{-3} L_\nu$ (Rosswog, Ramirez-Ruiz & Davies 2003), with the estimate $\dot{M}_b \sim L_{\nu\bar{\nu}} (GM_*/R_*)^{-1} \sim 5L_{\nu\bar{\nu}}/c^2$.

Powerful outflows can also be driven from accretion disks through magnetic fields. If the magnetic fields do not thread the BH, then a Poynting outflow can at most carry the gravitational binding energy of the torus. In this case, we may estimate their power

as (Blandford & Payne 1982):

$$L_{\text{MHD}} = \frac{B^2 r^3 \Omega}{2} \approx 10^{52} \text{ erg s}^{-1}, \quad (8)$$

where we have assumed that the field energy is at 10% of equipartition with the internal energy, ρc_s^2 , and typical values at the marginally stable orbit for calculations with $\dot{M} = 0.5 M_\odot \text{ s}^{-1}$ and $l_0 \approx 2 r_g c$ ($\rho \approx 10^{10} \text{ g cm}^{-3}$, $kT \approx 5 \text{ MeV}$). However, if the more massive central black hole is rapidly spinning, its larger energy reservoir is in principle extractable through MHD coupling to the disk by the Blandford & Znajek (1977) mechanism. These are clearly very rough estimates as none of these effects is explicitly included in our calculations, but it is clear that the large densities obtained even with modest values of the equatorial angular momentum allow in principle substantial magnetic fields to be anchored in the flow. Recent numerical MHD calculations assuming both adiabatic and neutrino-cooled flows in collapsing envelopes do show these general features (Proga & Begelman 2003b; Mizuno et al. 2004; Proga 2005; McKinney 2005; De Villers, Staff & Ouyed 2005).

Strong winds from hypercritical accretion flows may play an important role in the production and morphology of supernovae and γ -ray bursts. In the first place, the corresponding energy, however transferred to the outer layers, may actually explode the star and power the supernova explosion itself (MacFadyen & Woosley 1999; MacFadyen 2003; Thompson, Quatern & Burrows 2005). Second, the toroidal geometry inherent in flows endowed with angular momentum will break the spherical symmetry, and allow for higher efficiency than purely radial inflow in terms of liberating the gravitational energy in the system. Asymmetries may be reflected in the explosion itself and its remnant or in the beaming of a possible γ -ray burst, and can be quantified through line profiles (Mazzali et al. 2005) and collimation of the outflow (Panaitescu & Kumar 2001). Third, if the accretion flow cools inefficiently because it becomes so dense that the internal energy is simply advected into the black hole (Lee, Ramirez-Ruiz & Page 2004; Janiuk et al. 2004; Lee, Ramirez-Ruiz & Page 2005), it is possible that strong winds may actually revive the stalled accretion shock and make it reach the stellar envelope (Kohri, Narayan & Piran 2005). The argument is analogous to that invoked for classical Advection Dominated Accretion Flows, or ADAFs (Narayan & Yi 1994), except that the processes involve neutrino, instead of radiative cooling. Finally, the nucleosynthesis in such winds has been the focus of a number of recent studies, particularly in what concerns the production of r -process elements (Pruet, Thompson & Hoffman 2004).

The observable consequences are thus potentially far-reaching, and will be intimately connected with the processes occurring in the innermost regions of the flow. As we have shown here, a crucial ingredient in this respect is the angular momentum of the accreting gas, even at values that are usually considered to be too low in terms of the dynamics and the associated energy release.

4. DISCUSSION

Spherical accretion flows on to black holes have in general low radiative efficiencies, and this applies regardless of the cooling mechanism. If the flow is slightly rotating, the situation changes dramatically. Much of our effort in this work is therefore dedicated to determining the state of the gas falling quasi-spherically onto stellar-mass black holes with accretion rates in the range $10^{-3} \lesssim \dot{M} \lesssim 0.5 M_\odot \text{ s}^{-1}$. In this hypercritical regime, the gravitational accretion energy is carried away by neutrinos (Chevalier 1989).

Whether a disk forms or not depends on the precise value of the angular momentum, which is difficult to calculate as it depends on the physics of angular momentum transport inside the progenitor star. An approximate condition for disk formation is that the specific angular momentum of the infalling gas l exceeds $r_g c$. In most previous discussions, it has been assumed that $l \gg r_g c$ in order for a black hole to switch onto a luminous state. We argue here that flows in hyperaccreting, stellar mass disks around black holes are likely to transition to a highly radiative state when their angular momentum is just above the threshold for disk formation $l \sim 2 r_g c$. In this regime, a *dwarf* disk forms in which gas rapidly spirals into the black hole without any help from horizontal viscous stresses because of general relativistic effects. Such a disk is drastically different from its standard high- l counterpart as regards to its dynamics, energy dissipation and emitted spectrum.

It is extremely unlikely that the progenitors of GRBs are just very massive, single WR stars. Special circumstances are almost certainly needed. The prompt formation of a black hole can provoke the failure a core collapse supernova, if successfully shock breakout depends on delayed neutrino heating from the proto-neutron star. So perhaps one important distinction between a GRB and an ordinary supernova is whether a black hole or a neutron star is formed in the aftermath. However, not all black hole formation events can lead to a GRB: if the minimum mass of a single star that leads to the formation of a black hole is as low as $25 M_\odot$, this would overproduce GRBs by a large factor (see Izzard et al. 2004; Podsiadlowski et al. 2004).

The most widely discussed additional ingredient for GRB production is rotation: a rapidly rotating core is thought to be an essential ingredient in the collapsar model (Woosley 1993; MacFadyen & Woosley 1999). Massive stars are generally rapid rotators on the main sequence. However, there are well-established mechanisms, such as mass loss and magnetic torques, by which they can lose a substantial amount of angular momentum during their evolution. Thus, it is not at all clear whether the cores of massive single stars will ever be rotating rapidly at the time of explosion (e.g. Heger et al. 2005). The specific angular momentum l of the accreting core is thus a key ingredient. The simplest way to generate a high- l disk ($l \gg r_g c$) is for the core to reside in a tight binary and be in corotation with the binary. The requirement that the total core angular momentum exceed the maximum angular momentum of a Kerr black hole places interesting limits on the binary period (Izzard et al. 2004; Podsiadlowski et al. 2004). If we make the reasonable assumption that the binary is circular, and model the core as an $n = 3$ polytrope, the binary period must be smaller than $P_{\text{orb}} \sim 4(M_{\text{core}}/2M_\odot)^{-1}(R_{\text{core}}/10^{10} \text{ cm})^2 \text{ h}$. This orbit could be tight enough that the core may in fact have been stripped of its helium in a common envelope to form a CO core. By contrast, in most cases, the core of a massive, single star is unlikely to retain the required angular momentum as its outer hydrogen layers are blown off in a stellar wind. In this case, the accretion flows would be quasi-spherical with $l \sim r_g c$. While these progenitor models were previously excluded on grounds of low angular momentum, we suggest here that they should be reconsidered as valid candidates.

In fact, given the preferential range of l explored in this work, we argue that, as long as $l \geq 2r_g c$, low angular momentum cores may in fact be better suited for producing neutrino-driven explosions following massive core collapse.

We gratefully acknowledge helpful discussions with A. Heger, T. Janka, J. McKinney, P. Mészáros, D. Proga, M. Rees and S. Woosley. Financial support for this work was provided in part by CONACyT-36632E (W.H.L.) and NASA through a Chandra Postdoctoral Fellowship award PF3-40028 (E.R.-R.).

REFERENCES

- Akiyama, S., Wheeler, J. C., Meier, D. L., Lichtenstadt, I. 2003, *ApJ*, 584, 954
- Ardeljan, N. V., Bisnovatyi-Kogan, G. S., Moiseenko, S. G. 2005, *MNRAS*, 359, 333
- Beloborodov, A. M. & Illiaronov, A. F. 2001, *MNRAS*, 323, 167
- Bethe, H. A., Wilson, J. R. 1985, *ApJ*, 295, 14
- Blandford, R. D., Payne, 1982, *MNRAS*, 199, 883
- Blandford, R. D., & Znajek, R. L. 1977, *MNRAS*, 179, 433
- Burrows, A., Thompson, T. A. 2003, in "From Twilight to Highlight: The Physics of Supernovae", ESO Astrophysics Symposia, W. Hillebrandt, B. Leibundgut, eds., p.53
- Chen, X., Taam, R. E., Abramowicz, M. A., Igumenshchev I. V. 1997, *MNRAS*, 285, 439
- Chevalier, R. A. 1989, *ApJ*, 346, 847
- De Villiers, J.-P., Staff, J., Ouyed, R. 2005, preprint, astro-ph/0502225
- Fryer, C. L., Heger, A. 2000, *ApJ*, 541, 1033
- Fryer, C. L., Warren, M. S. 2004, *ApJ*, 601, 391
- Heger, A., Woosley, S. E., Spruit, H. C. 2005, *ApJ*, 626, 350
- Igumenshchev, I. V., Abramowicz, M. A. 1999, *MNRAS*, 303, 309
- Itoh, N., Adachi, T., Nakagawa, M., Kohyama, Y., & Munakata, H. 1989, *ApJ*, 339, 354 (erratum 360, 741 [1990])
- Izzard, R. G., Ramirez-Ruiz, E., Tout, C. A. 2004, *MNRAS*, 348, 1215
- Janiuk, A., Perna, R., Di Matteo, T., Czerny, B. 2004, *MNRAS*, 355, 950
- Janka, H.-Th., Müller, E. 1996, *A&A*, 306, 167
- Janka, H.-Th., Scheck, L., Kifonidis, K., Müller, E., Plewa, T. 2005, in "The Fate of the Most Massive Stars", ASP Conference Proceedings, vol. 332, R. Humphreys and K. Stanek, eds., p. 372
- Kohri, K. & Mineshige, S. 2002, *ApJ*, 577, 311
- Kohri, K., Narayan, R., & Piran, T. 2005, *ApJ*, 629, 341
- LeBlanc, J. M., Wilson, J. R. 1970, *ApJ*, 161, 541
- Lee, W. H. & Ramirez-Ruiz, E. 2002, *ApJ*, 577, 893
- Lee, W. H., Ramirez-Ruiz, E. & Page, D. 2004, *ApJ*, 608, L5
- Lee, W. H., Ramirez-Ruiz, E. & Page, D. 2005, *ApJ* in press
- MacFadyen A. I. 2003, in "From Twilight to Highlight: The Physics of Supernovae", ESO Astrophysics Symposia, W. Hillebrandt, B. Leibundgut, eds., p.97
- MacFadyen A. I., Woosley, S. E. 1999, *ApJ*, 524, 262
- Mazzali, P. et al. 2005, *Science*, 308, 1284
- McKinney, J. 2005, *ApJ*, 630, L5
- Mizuno, Y., Yamada, S., Koide, S., Shibata, K. 2004, *ApJ*, 615, 389
- Narayan, R., Yi, I. 1994, *ApJ*, 428, L13
- Narayan, R., Piran, T. & Kumar, P. 2001, *ApJ*, 557, 949
- Paczynski, B. & Wiita, P.J. 1980, *A&A*, 88, 23
- Panaiteescu, A. & Kumar, P. 2001, *ApJ*, 554, 667
- Podsiadlowski, Ph., Mazzali, P. A., Nomoto, K., Lazzati, D., Cappellaro, E. 2004, *ApJ*, 607, L17
- Popham, R., Woosley, S. E. & Fryer, C. 1999, *ApJ*, 518, 356
- Proga, D. 2005, *ApJ*, 629, 397
- Proga, D., MacFadyen, A. I., Armitage, P. J., Begelman, M. C. 2003, *ApJ*, 599, L5
- Proga, D. & Begelman, M. C. 2003a, *ApJ*, 582, 69
- Proga, D. & Begelman, M. C. 2003b, *ApJ*, 592, 767
- Pruet, J., Thompson, T. A., & Hoffman, R. D. 2004, *ApJ*, 614, 847
- Qian, Y.-Z. & Woosley, S.E. 1996, *ApJ*, 471, 331
- Ramirez-Ruiz, E., Socrates, A. 2005, *ApJ* submitted (astro-ph/0504257)
- Rosswog, S., Ramirez-Ruiz, E. & Davies M. B. 2003, *MNRAS*, 345, 1077
- Shapiro, S. A. & Teukolsky, S. L. 1983, *Black Holes, White Dwarfs and Neutron Stars*, Wiley Interscience, NY
- Spruit, H. C. 2002, *A&A*, 381, 923
- Thompson, T. A., Quataert, E., Burrows, A. 2005, *ApJ*, 620, 861
- Wilson, J. R., Mathews, G. J., Dalhed, H. E. 2005, *ApJ*, 628, 335
- Wheeler, C. J., Meier, D. L., Wilson, J. R. 2002, *ApJ*, 568, 807
- Woosley, S. E. 1993, *ApJ*, 405, 273
- Woosley, S. E., Heger, A. 2005, *ApJ* submitted (astro-ph/0508175)
- Yoon, S.-C., Langer, N. 2005, *A&A* submitted (astro-ph/0508242)

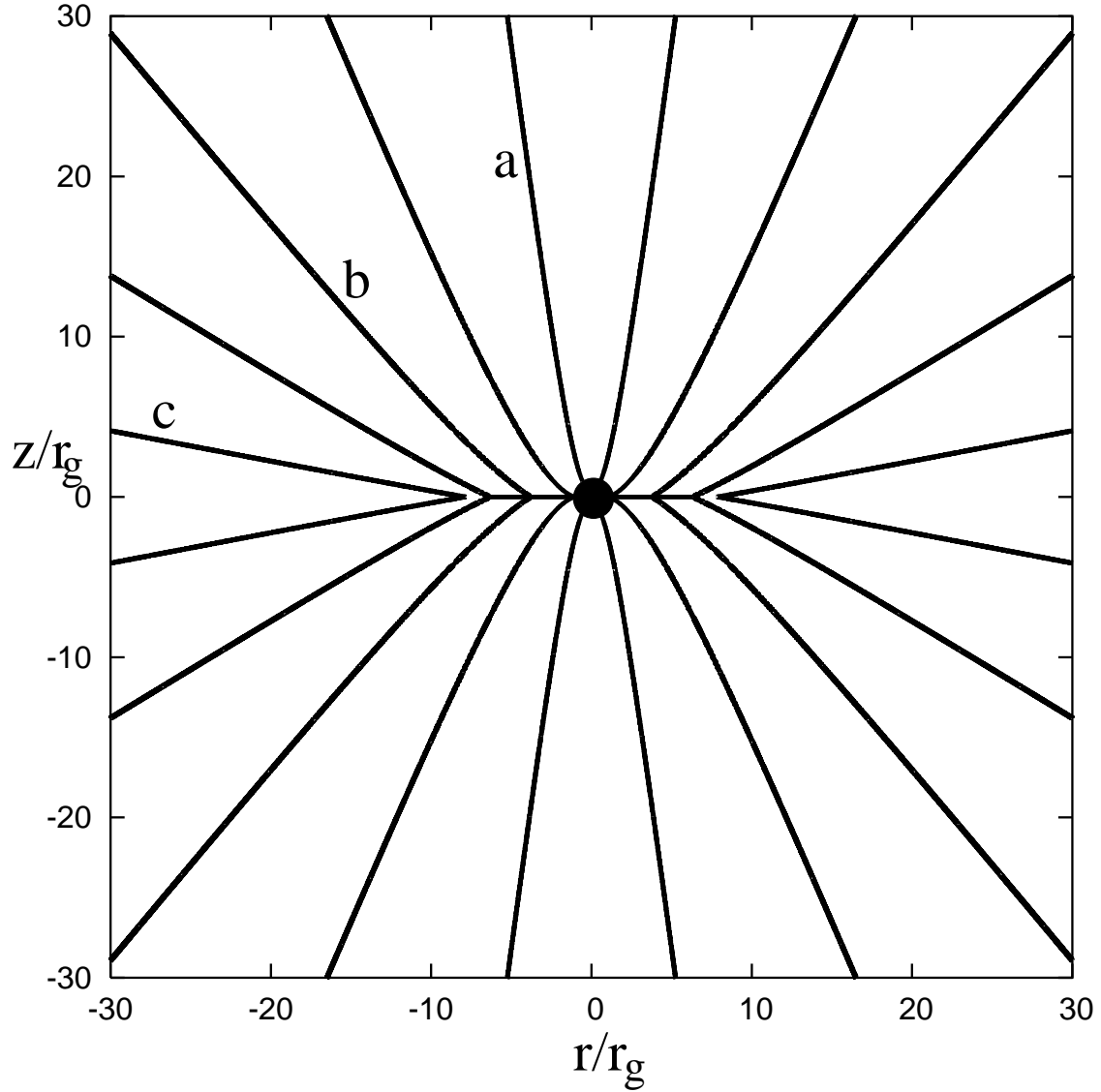


FIG. 1.— Flow lines for ballistic, nearly parabolic motion of particles surrounding a black hole of mass M and rotating about a given axis, z , with angular frequency Ω . It is assumed that the specific angular momentum, l , increases monotonically with the polar angle θ , and that flow lines do not intersect before reaching the equator. The particular lines drawn here are for rigid body rotation, with $l = l_0 \sin^2 \theta$. Lines of type (a) directly impact the black hole, those of type (b) would do so as well if they did not cross the equator first, while those of type (c) have enough angular momentum to remain in equatorial orbit at a finite radius r . If the energy in vertical motion is dissipated efficiently, a thin inviscid disk will form in the equatorial plane, denoted by a thick line.

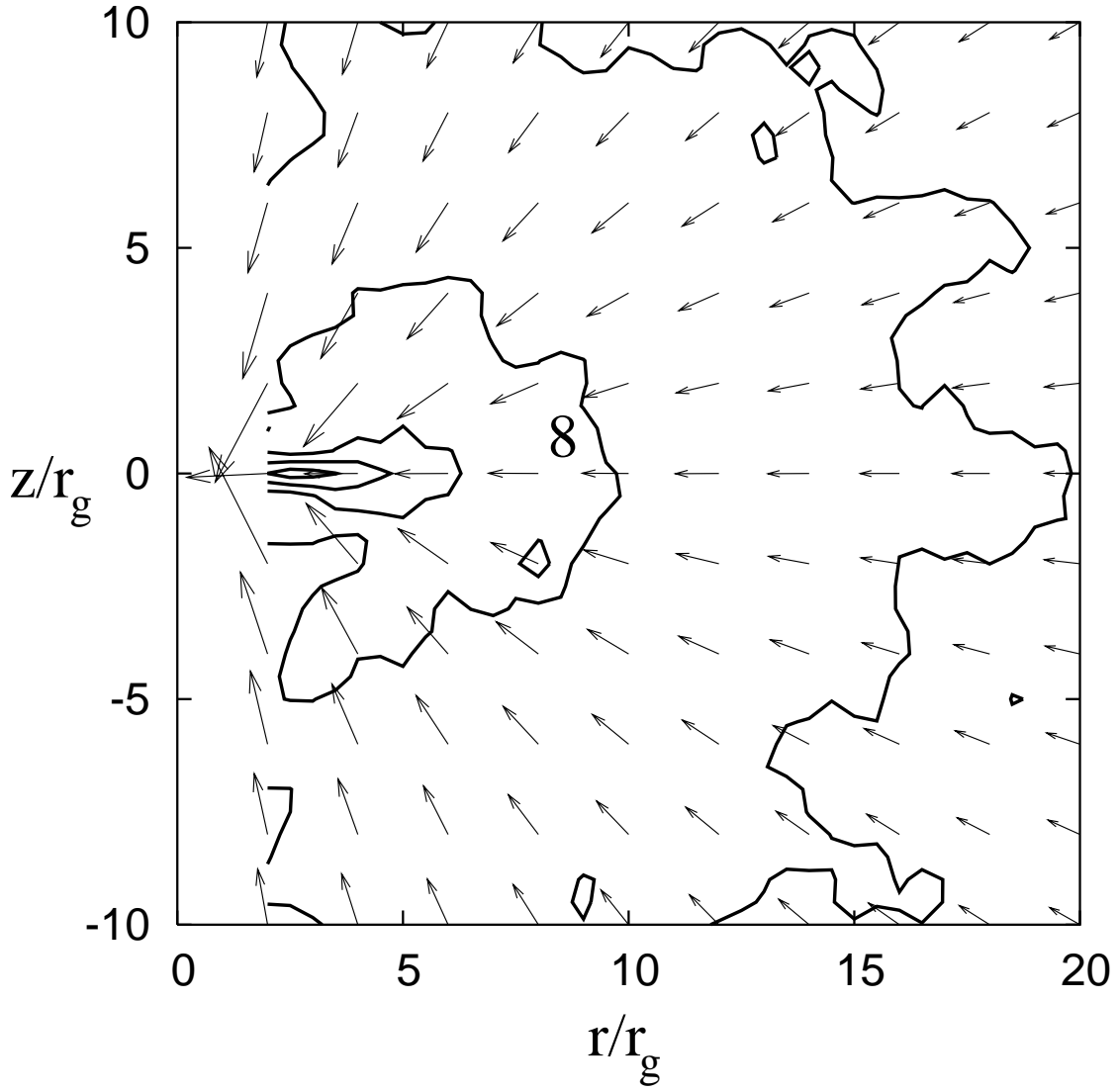


FIG. 2.— Logarithmic density contours and velocity field in the meridional plane for a low angular momentum calculation ($l_0 = 1.9r_gc$). The accretion rate is $\dot{M} = 0.5 M_\odot \text{ s}^{-1}$. The flow is steady and the character of the solution is independent of the adopted value of the viscosity parameter α and the accretion rate. Only a thin dwarf equatorial disk is present at small radii. The contours are evenly spaced every 0.5 dex and labeled in g cm^{-3} .

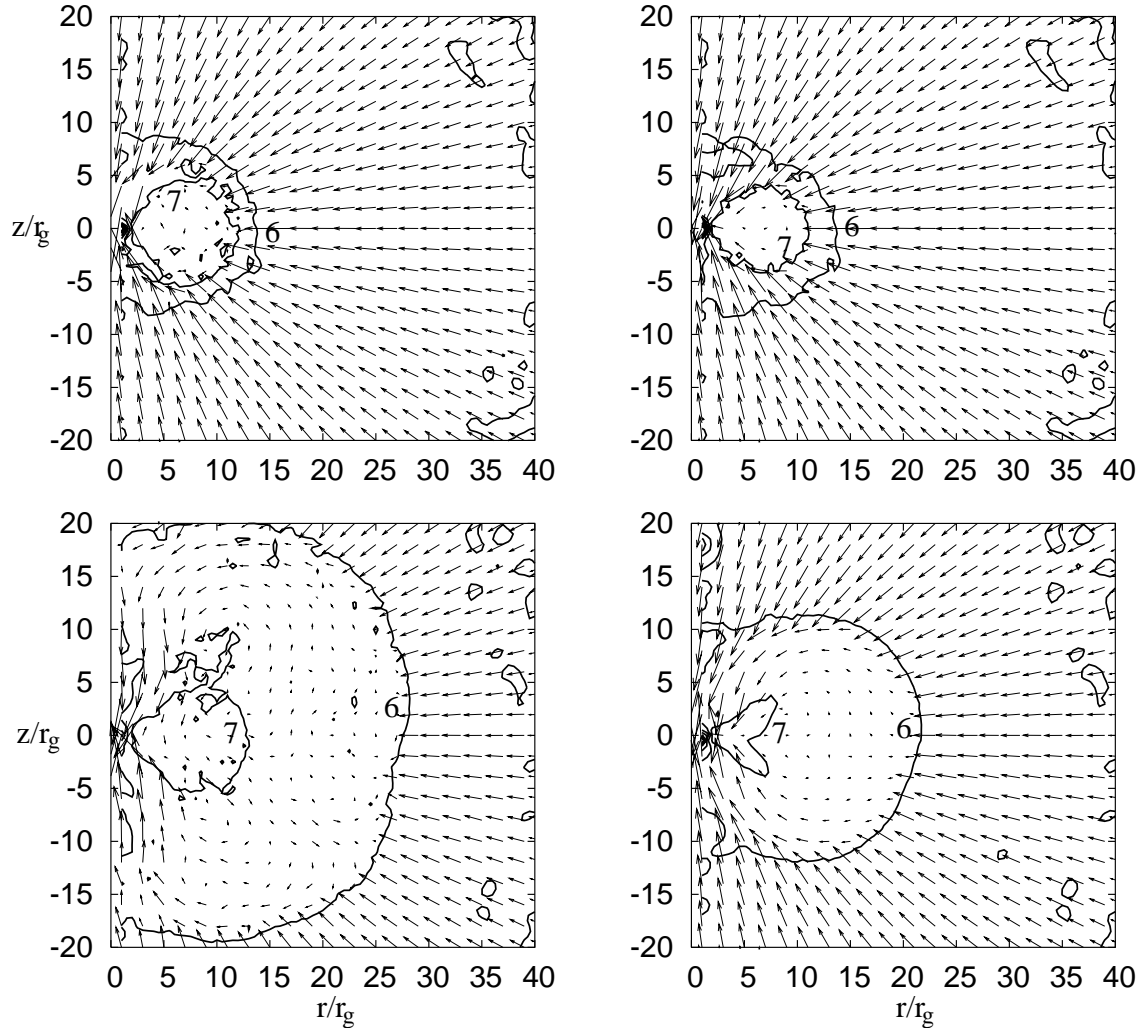


FIG. 3.— Logarithmic density contours and velocity field in the meridional plane for high angular momentum calculations ($l_0 = 2.1 r_g c$), with $\alpha = 0$ (left column) and $\alpha = 0.1$ (right column), at $t = 500 r_g / c$ (top row) and $t = 1500 r_g / c$ (bottom row). The accretion rate is $\dot{M} = 0.01 M_\odot \text{ s}^{-1}$. In both cases the hot toroidal bubble grows continuously as the shock front moves outward, but it is clearly smaller in the high-viscosity case. The contours are evenly spaced every dex and labeled in g cm^{-3} .

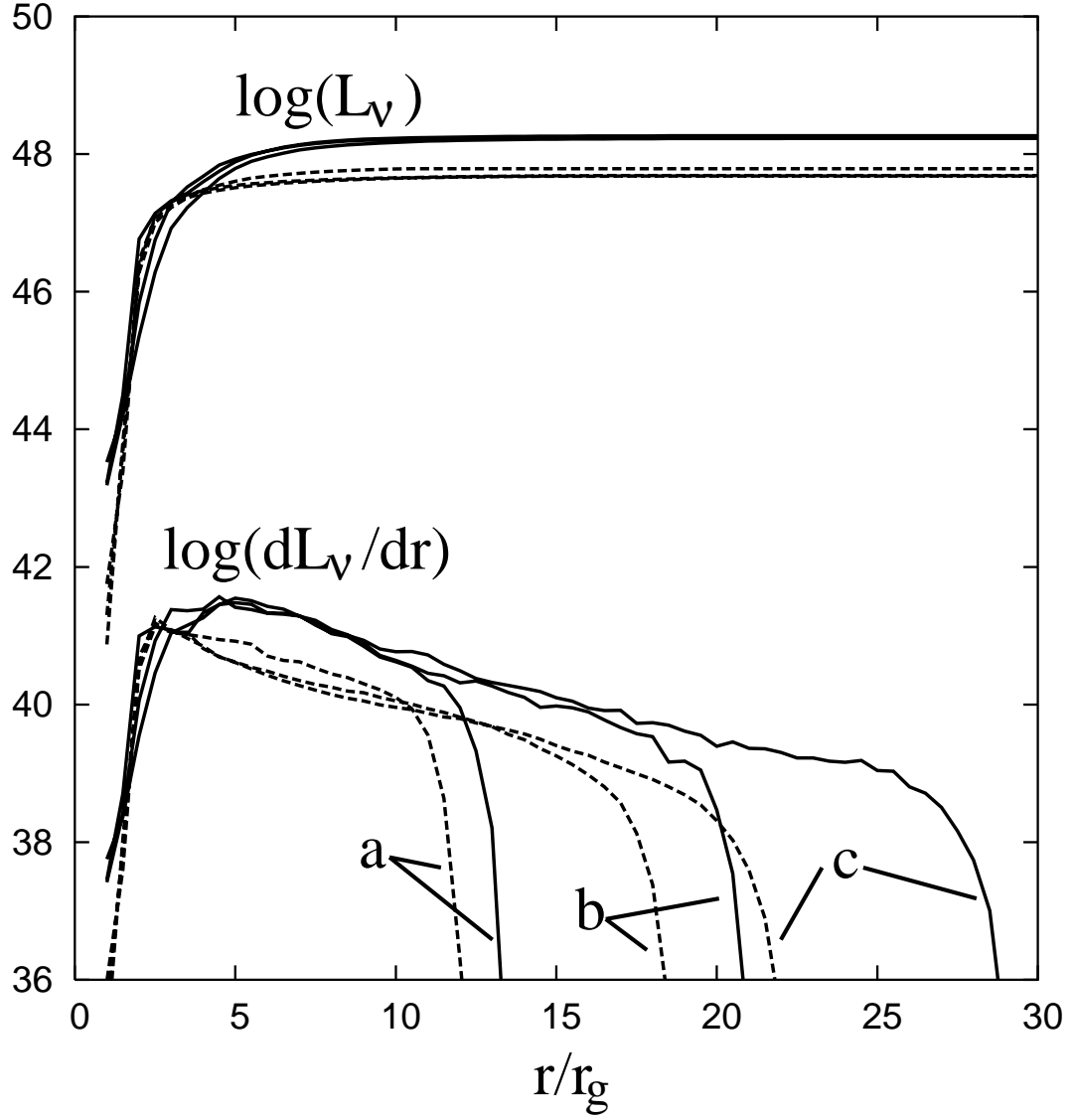


FIG. 4.— Neutrino luminosity per radial interval, dL_ν/dr (lower lines), in $\text{erg cm}^{-1} \text{s}^{-1}$, as a function of radius at (a) $t = 500r_g/c$, (b) $t = 1000r_g/c$, and (c) $t = 1500r_g/c$ for high-angular momentum calculations ($l = 2.1r_gc$) without ($\alpha = 0$, solid lines) and with ($\alpha = 0.1$, dashed lines) viscosity, for $\dot{M} = 0.01 M_\odot \text{s}^{-1}$. The corresponding solid and dashed lines above show the integrated luminosity L_ν in erg s^{-1} . The outward motion of the shock is clearly visible in the sharp drop in emissivity as the calculation progresses.

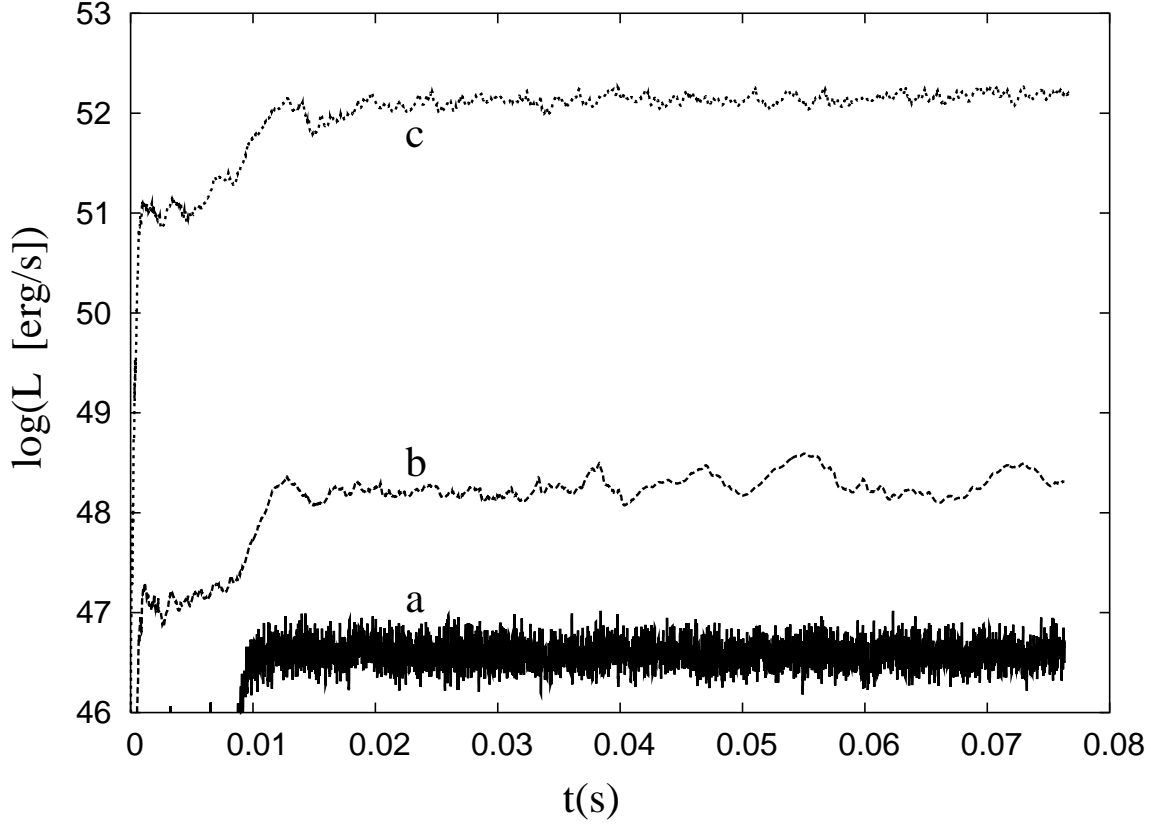


FIG. 5.— Neutrino luminosity L_ν in erg s^{-1} as a function of time for inviscid ($\alpha=0$) runs with (a) $l_0 = 1.9r_g c$, $\dot{M} = 0.01 M_\odot \text{ s}^{-1}$; (b) $l_0 = 2.1r_g c$, $\dot{M} = 0.01 M_\odot \text{ s}^{-1}$; (c) $l_0 = 2.1r_g c$, $\dot{M} = 0.5 M_\odot \text{ s}^{-1}$. For low angular momentum it is essentially steady, although strong variability around a steady average is apparent. For high angular momentum, high amplitude, quasi-periodic variations are seen as a result of large-scale variations in the size and shape of the hot toroidal bubble.

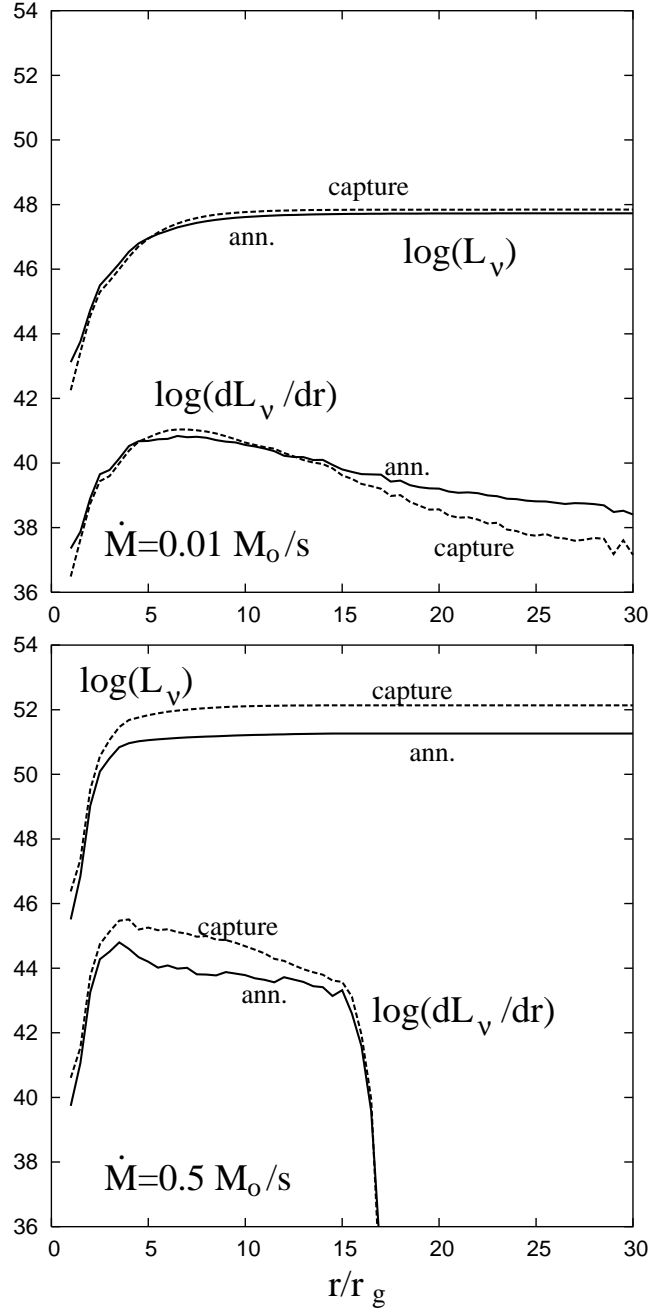


FIG. 6.— Same as Figure 4, but for $l = 2.2r_g c$ and $\alpha = 0$. Calculations with $\dot{M} = 0.01 M_\odot s^{-1}$ (top) and $\dot{M} = 0.5 M_\odot s^{-1}$ (bottom) are shown at $t = 1500r_g c$. The solid (dashed) lines show the contribution from pair annihilation (pair capture onto free nucleons) to the total luminosity. At high accretion rates pair capture dominates the cooling and makes the hot toroidal bubble smaller.

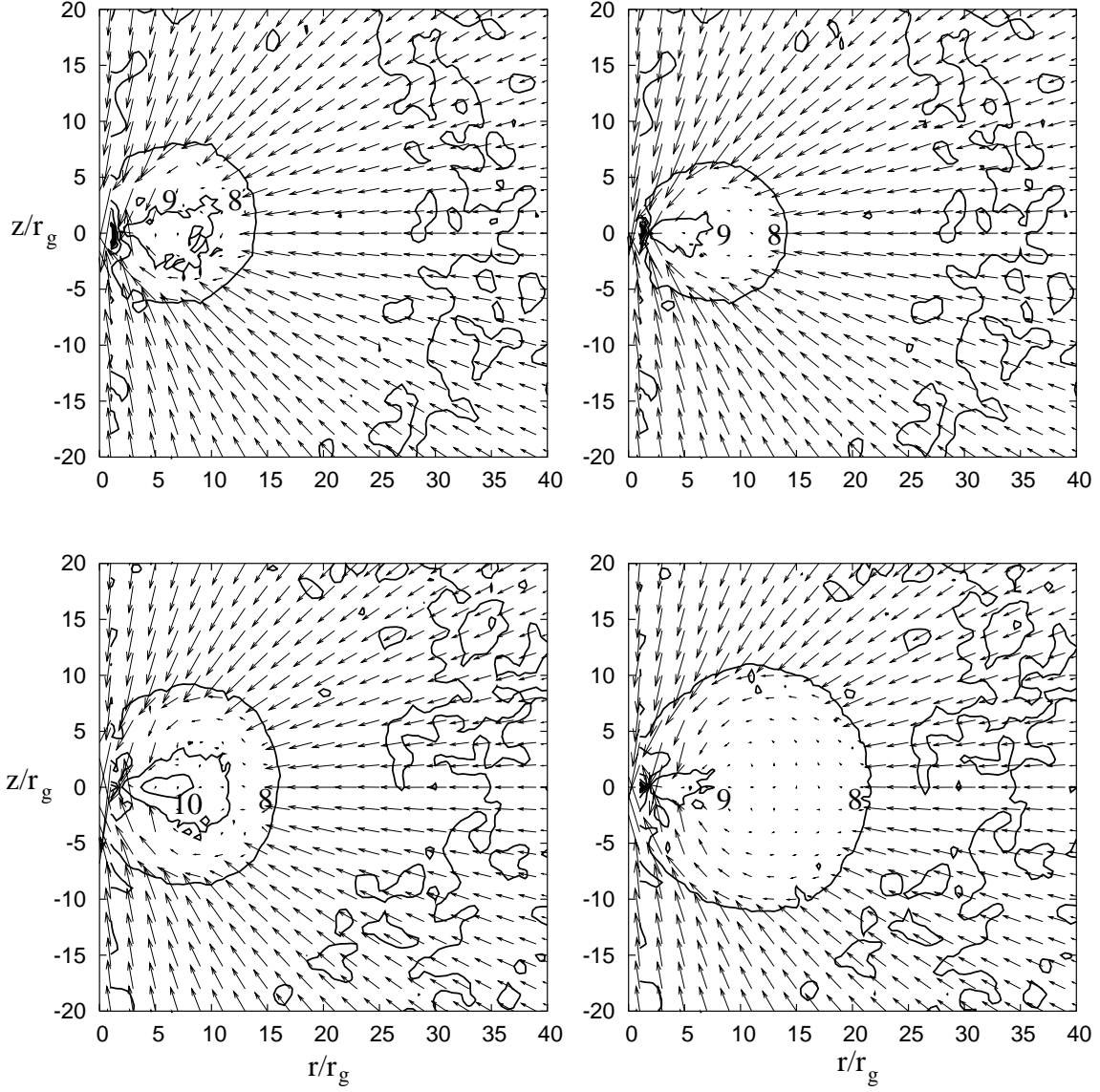


FIG. 7.— Same as Figure 3 but for $\dot{M} = 0.5 M_{\odot} \text{ s}^{-1}$ and $l_0 = 2.1 r_g c$. As before, the hot toroidal bubble grows as the shock front moves outward, but this time, as opposed to the case of low accretion rate, it is clearly smaller in the inviscid case. The contours are evenly spaced every dex and labeled in g cm^{-3} .

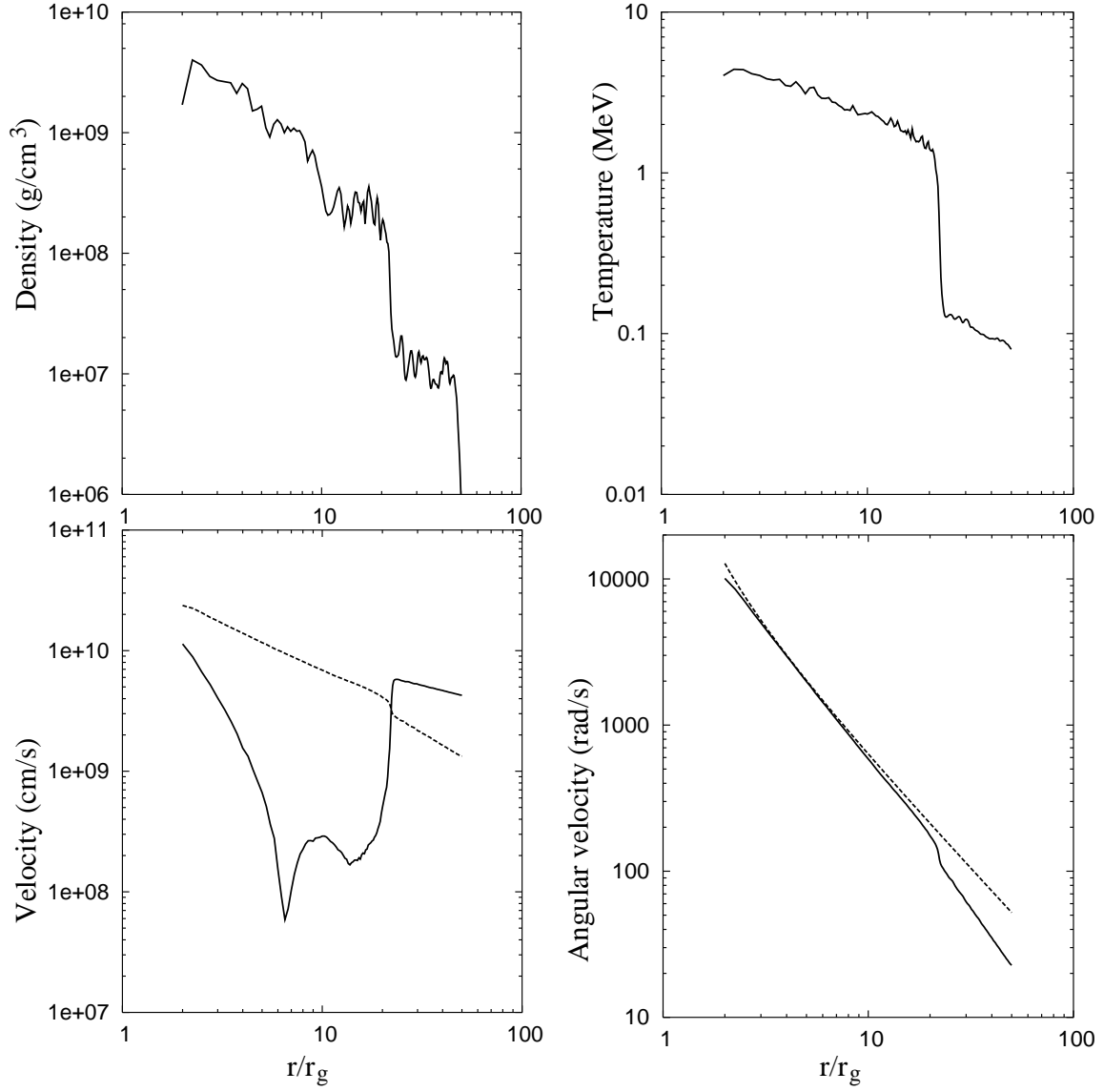


FIG. 8.— Density, temperature and velocities along the equator, $z = 0$, for the calculation with $l_0 = 2.2r_g c$ and $\alpha = 0.1$ at late times, when the toroidal bubble has stabilized. In the bottom left panel, the solid (dashed) line is for the radial (azimuthal) component of the velocity. The bottom right panel shows the computed angular velocity (solid line) as well as the Keplerian solution in the Paczynski–Wiita potential for reference (dashed line).

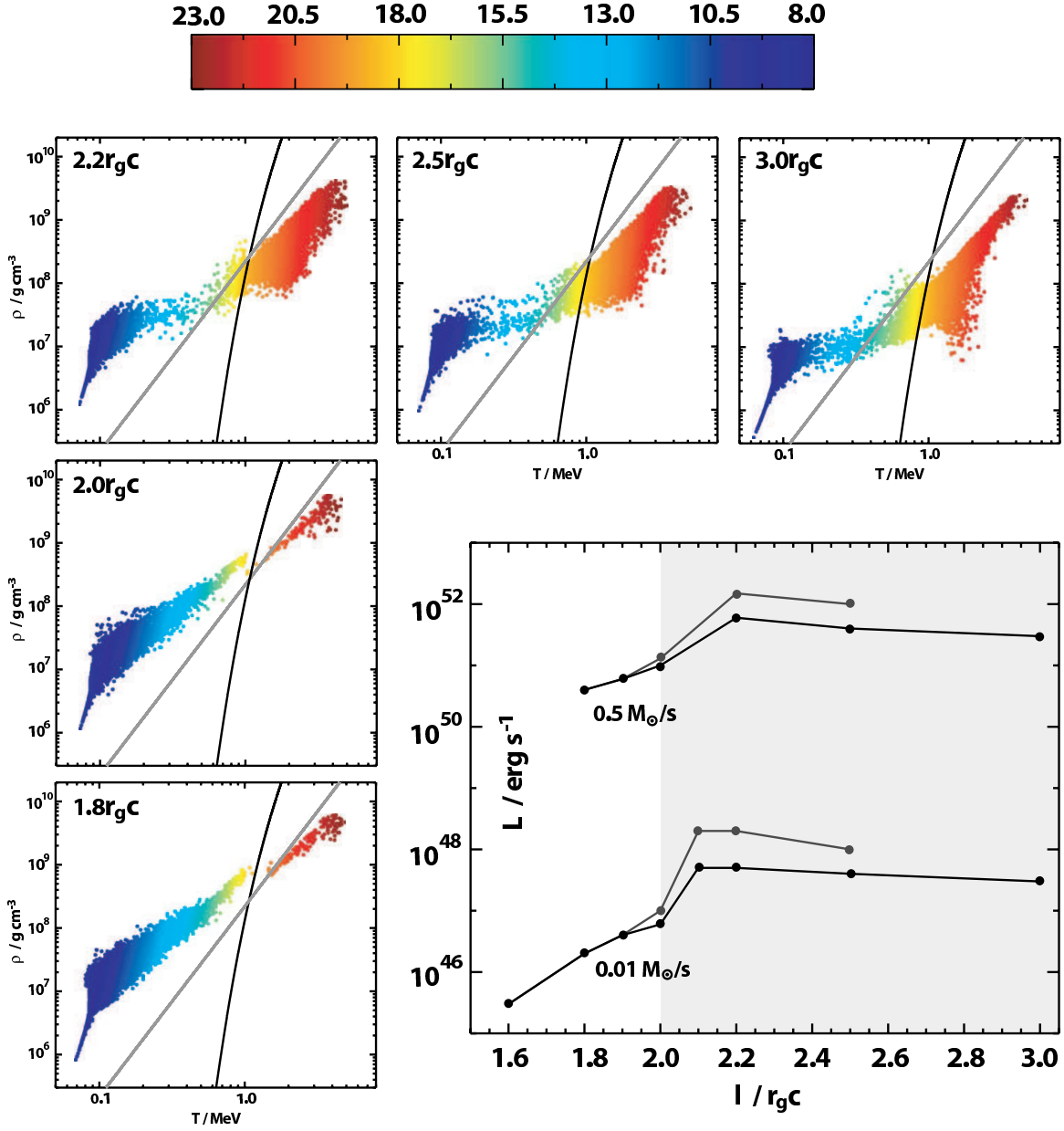


FIG. 9.— Flow structure in the density–temperature plane for calculations with varying equatorial angular momentum l_0 (labeled) at $\dot{M} = 0.5 M_\odot \text{ s}^{-1}$ and color coded according to the volume cooling rate (in $\text{erg cm}^{-3} \text{ s}^{-1}$). The black and grey solid lines across each plot show the degeneracy ($kT = 7.7 \rho_{11}^{1/3} \text{ MeV}$) and photodisintegration of (50% of α particles into free nucleons by mass) thresholds respectively. The transition from a dwarf disk to a hot toroidal bubble as l_0 increases beyond $\simeq 2.1 r_g c$ is clearly seen, as is the slight decrease in maximum density at high angular momentum. The characteristic neutrino luminosity is plotted in the large panel as a function of l_0 for two different mass accretion rates, and viscous ($\alpha = 0.1$, black lines) and inviscid calculations ($\alpha = 0$, gray lines). The qualitative change in the dependence of L_ν on l_0 occurs around $2.1 r_g c$. Note that at high accretion rates, even low angular momentum configurations ($l_0 \simeq 1.8 r_g c$) are capable of releasing up to $10^{51} \text{ erg s}^{-1}$.

TABLE 1
NEUTRINO ENERGIES AND MAXIMUM DENSITIES^a

$l_0/(r_g c)$	$E_\nu^{\text{pair}}(\text{MeV})$	$E_\nu^{\text{ann.}}(\text{MeV})$	$\rho_{\text{max}}(\text{g cm}^{-3})$	$kT(\text{MeV})$
2.1	11	3	3×10^{10}	3
2.2	11	3	3×10^{10}	3
2.5	5	3	3×10^9	3
3.0	4	3	2×10^9	3

^aFor all the runs shown here, $\alpha = 0$ and $\dot{M} = 0.5 \text{ M}_\odot \text{ s}^{-1}$.